A Search for Flaring Very-High-Energy Cosmic γ-ray Sources with the L3+C Muon Spectrometer

The L3 Collaboration

Abstract

The L3+C muon detector at the CERN electron-positron collider, LEP, is used for the detection of very-high-energy cosmic γ-ray sources through the observation of muons of energies above 20, 30, 50 and 100 GeV. Daily or monthly excesses in the rate of single-muon events pointing to some particular direction in the sky are searched for. The periods from mid July to November 1999, and April to November 2000 are considered. Special attention is also given to a selection of known γ-ray sources. No statistically significant excess is observed for any direction or any particular source.

1 Introduction

The energy spectrum of cosmic rays spans a very broad range, from sub-GeV to energies larger than 10^{11} GeV. No single mechanism of particle production and acceleration at any astrophysical site can still explain this remarkable feature. However, the fact that the energy spectrum has a relatively smooth power law shape over 11 decades in energy with two pronounced features, the *knee* at $\sim 3 \times 10^{15}$ eV and the *ankle* at $\sim 3 \times 10^{18}$ eV, strongly suggests some generic relationship between particles of different energies. A reasonably detailed understanding of the origin, acceleration and propagation of low energy cosmic rays in the galactic disk has evolved over the recent years, thanks to very detailed and accurate measurements of elemental and isotopic abundances at sub-GeV and GeV energies. With the results available from satellite-borne detectors on cosmic γ-rays, significant progress is being made in our knowledge of cosmic ray sources at GeV energies [1]. However, studies at energies > 100 GeV are very difficult with satellite-based detectors due to practical constraints on detector size and exposure factor. Though attempts have been made to detect sources at TeV energies using the atmospheric Cherenkov radiation since late 1950's, significant progress in the detection of sources has been made only after the successful development and application of imaging techniques. Among the sources so far detected are supernova remnants, pulsars, X-ray binaries, active galactic nuclei, and as more recently discovered, a starburst- and a radio-galaxy. Most of the presently operational imaging telescopes have a detection energy threshold above ~ 150 to 300 GeV. Larger telescopes with improved electronics and imaging resolution are being designed and just start operation. These will work with a reduced energy threshold of a few tens of GeV, which helps in bridging the wide energy gap between the observations with satellite-borne detectors and Cherenkov telescopes [2–5].

Observational studies with both these techniques, the γ-ray telescope aboard space-borne platforms at GeV energies and the atmospheric Cherenkov telescope at TeV energies, are constrained by the fact that a given telescope can observe only a single source at a given time. In addition, the duty factor of the Cherenkov telescope is severely limited to ≤ 8 % due to the requirement of moon-less and fog-less nights for observations. On the other hand, the air shower technique offers the advantage of daily observations spread over $5-6$ hours on all sources within a well-defined declination band accessible at the specific observational site. However, the fact that the arrival angle of a shower can be determined accurately only for relatively large showers pushes the threshold for γ-ray detection to energies higher than $\sim 10^{14}$ eV [6]. Detectors with very large sensitive area such as MILAGRO [7] are now attempting to reduce the energy threshold of 'air shower' type detectors to TeV energies.

A high-energy muon tracking detector has the same advantage as the air shower detector in terms of its daily coverage of all sources within a well-defined declination band. However, the sensitivity of a muon tracking-detector is significantly smaller for detection of cosmic γ-rays due to the very small cross-section for photo-production of charged pions in interaction of γ-rays with air nuclei [8]. This disadvantage is partially offset by the fact that the muon tracking-detector can have a lower energy threshold, even lower than the presently operational Cherenkov telescopes, if located at a shallow depth underground. Therefore, muon tracking-detectors can be used with some advantage in survey-type experiments, particularly for flaring sources. Observations of intense bursts at TeV energies from the AGN's, Mkn 421 and Mkn 501, have highlighted this aspect of cosmic γ-ray sources in recent years [9].

The astrophysical significance of observations with the muon tracking detectors was emphasized by the Soudan I experiment [10] in 1985 when it reported observation of a 4.8 hr modulated

signal in the flux of muons ($E_\mu > 650$ GeV) arriving from the direction of the powerful X-ray binary, Cygnus X-3. A similar observation was reported by the NUSEX collaboration [11] with muons of energy ≥ 1.3 TeV. The assumption that the primary was a γ was also questioned. While several detections, each with relatively low statistical significance, were reported in the 1980's at TeV, PeV and EeV energies for Cygnus X-3 [12], no group has reported detection of a signal from Cygnus X-3 in the 1990's and later [13–15], except SOUDAN II in 1991 [16]. These observations may be interpreted in terms of an active phase for the source in the 1980's and highlight the importance of monitoring the sky for flaring sources at different energies and times [17].

The unique properties of the L3+C muon spectrometer [18, 19], offer a new opportunity to search for large flares from known, as well as yet unknown sources at relatively low energies at about $100-1000$ GeV. This reach is also due to the location at a shallow depth when compared to other underground detectors such as MACRO [20]. The ability to select a muon energy threshold with the L3+C muon spectrometer makes it possible to optimize the signal-to-background ratio. It may be noted that observations of muons with L3+C have a threshold energy sensitivity of about 100 GeV to cosmic γ-rays, an energy range not yet well explored by Cherenkov telescopes, and up to now not accessible to space-borne γ-ray detectors . Based on the flux of γ-rays derived from Cherenkov telescopes measurements [6] steady source signals are not expected to be observed with the L3+C detector.

The L3+C muon spectrometer and the data taking are presented in the next section. In section 3 we discuss the angular resolution of the L3+C muon spectrometer, the procedure for the binning of the data and the determination of the background. The results obtained for some interesting astrophysical sources are given in section 4, and a survey of the entire sky accessible to L3+C in section 5. The conclusions drawn from these observations are presented in the last section.

2   The L3+C Muon Spectrometer

The L3 detector (Figure 1) [18, 19] was designed to accurately measure muons, electrons, photons and hadrons at the large electron positron collider, LEP, at CERN. It consisted of a huge solenoidal magnet of 1000 m^3 volume with a field of 0.5 T and a set of high precision drift chambers arranged in octants. At 45 GeV/c the momentum resolution is 4.6 % for muons measured in one chamber octant only. This has been determined from muons from the decay of Z bosons [19] produced in e$^+$e$^-$ interactions of LEP. The vertex detectors, electromagnetic and hadronic calorimeters located in the central region of the L3 detector have not been used for the cosmic-ray study. The addition of scintillators on the top of the magnet, which provided the arrival time of muons, as well as separate trigger and readout electronics, enabled the acquisition of cosmic muons independent of the running of the L3 experiment and LEP. The constancy of the efficiency of all scintillator modules was monitored carefully, and the stability of the efficiency and accuracy of the reconstruction of muon tracks was checked as a function of time [21]. Chamber, scintillator, and trigger efficiencies have been discussed in detail elsewhere [22]. The arrival time of an event was recorded with an accuracy of 1 μsec (GPS timing). Periods with instabilities or noise induced by the operation of the LEP machine are excluded from the analysis, which is supplemented by a final 10-day run taken after the LEP accelerator had been stopped, in order to understand the influence of synchrotron radiation and other LEP-related backgrounds.

The spectrometer is located under only 30 m of overburden, and the energy threshold for

cosmic muons is about 15 GeV. The coordinates of the L3+C site are 6.02° E and 46.25° N, and the altitude is 450 m above sea level. Data were taken during two periods, mid-July to November in 1999 and April to November in 2000. Overall, 1.2×10^{10} triggers were recorded, for an effective live-time of 312 days.
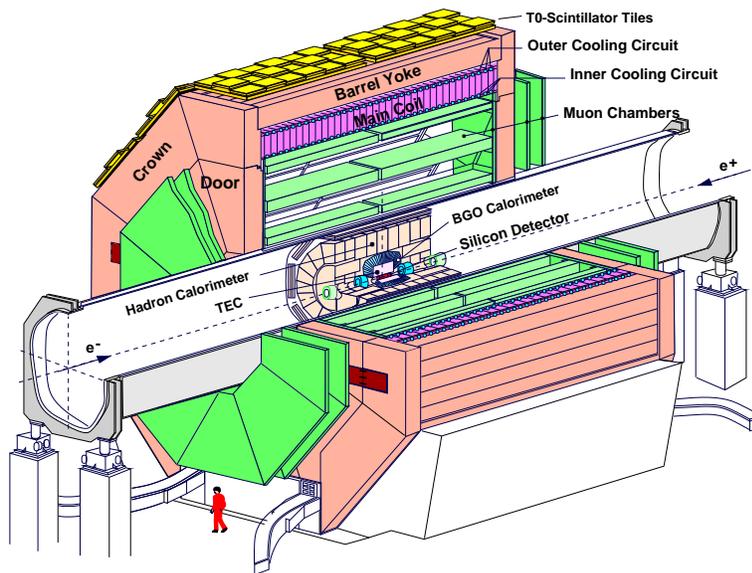
Figure 1: The L3 detector covered with the scintillators installed for timing cosmic-ray muons.

3   Search for Cosmic γ-ray Sources

The muon rate is determined as a function of the right ascension along thin declination bands. The direction-dependent intensity of primary particles Φ is assumed to be the sum of an isotropic part (background) and the contribution of a few discrete sources (signal) with declination δ_k and right ascension α_k:

$$\Phi(\delta, \alpha, E_0) = \sum_i \overline{\Phi_i}(E_0) + \sum_k \phi_k(E_0) \frac{D(\delta - \delta_k) \, D(\alpha - \alpha_k)}{\cos \delta_k} \tag{1}$$

where $\overline{\Phi_i}(E_0)$ is the isotropic background intensity of primary of type i of energy E_0 obtained through an integration:

$$\overline{\Phi_i}(E_0) = \frac{1}{4\pi} \int \Phi_i(\delta, \alpha, E_0) \mathrm{d}\Omega, \tag{2}$$

D is the Dirac δ-function and $\phi_k(E_0)$ is the intensity of the k-th point source of neutral particles, here assumed to be γ-rays. However, in an actual observation, the flux of particles due to a source cannot be represented by a Delta-function due to the finite angular resolution of the telescope. Therefore $\Phi(\delta, \alpha, E_0)$ has to be convoluted with the angular resolution $S(\Delta\theta, E_0)$, which represents the expected distribution of the angular difference $\Delta\theta$ between the direction of the primary particles with energy E_0 and the measured direction of the muons generated by them. It includes the effect of multiple scattering in the overburden and the angular reconstruction accuracy of the detector. The dependence of S on the direction (δ, h) (h is the

4

negative hour angle, equal to $\alpha - t_s$, and t_s is the sidereal time) has been neglected here (see below) and the normalization is chosen so that

$$\int S(\Delta\theta, E_0)\mathrm{d}\Omega = 1. \qquad (3)$$

The number $N_{\mathrm{tot}}^{\mathrm{bkg}}(\delta, \alpha; E_{\mathrm{cut}})$ of muons above a fixed energy threshold E_{cut} expected from the isotropic (background) component of the primary flux and detected originating from a given right ascension α and declination δ can be obtained, taking into account the detector's live-time distribution as a function of the sidereal time, the direction- and time- dependent detection efficiency as well as atmospheric effects [21].

3.1 Angular Resolution and Pointing Accuracy

The angular resolution of the detector itself is assured to be better than a milliradian due to the use of precision drift chambers. The effective angular resolution of the muon telescope is determined by two factors, namely the opening angle of the photo-produced pion in the γ-air nucleus interaction, a marginal effect according to Monte-Carlo estimations [23, 24] at the energies of interest here, and, most important, the zenith angle dependent scattering of the muon in the $\sim$ 30m-thick layer of molass (sedimentary rock) above the muon spectrometer. The angular resolution for the detected muon is first estimated from Monte Carlo simulations based on GEANT 3 [25] by comparing the direction of the muon with the direction reconstructed after taking into account the multiple scattering in the molass and the instrumental accuracies. Figure 2 shows distributions of the angle between the generated and reconstructed angle directions for muons above 30 GeV as an example, and for sets of different ranges of zenith angles, as well as for all accepted zenith angles. Figure 3 displays again the angular difference of incoming muons above 30 GeV and the outgoing muons, but for a set of declination angles integrated over the whole range of accepted zenith angle. This second plot shows that the angular bin size selected for a given muon energy is only weakly dependent on the source position for the given detector conditions (see below).

The muon angular resolution has also been estimated experimentally from the measurement of the angular difference $\theta_{2\mu}$ between muons from events containing two high energy muons. The excellent agreement of the results obtained from detailed Monte Carlo simulations with the observed $\theta_{2\mu}$ distribution allowed an estimate of the angular resolution for single muons. These estimates of angular resolution have been confirmed by the observation of a deficit in the flux of muons due to the shadowing of the cosmic ray flux by the Moon [26, 27]. A detailed simulation of the shadowing, including the deflection of protons in the geomagnetic field, has also confirmed the absolute pointing accuracy of the L3+C muon telescope to be better than $0.1°$ and the angular resolution to be $0.2°$ for muons of energy above 100 GeV. Simulations have further shown that muons produced by high energy γ-rays deviate e.g. by less than $\sim 0.3°$ from the primary γ-ray direction for muon energies above 40 GeV.

3.2 Angular Bin Size

The search for cosmic γ-ray sources has been carried out by using square bins in right ascension and declination. Since the angular resolution of the detection depends on the muon momentum, the optimal bin sizes for various momentum thresholds have also been determined from simulations. For a pure Gaussian-shaped angular resolution with standard deviation $\sigma°$, it has
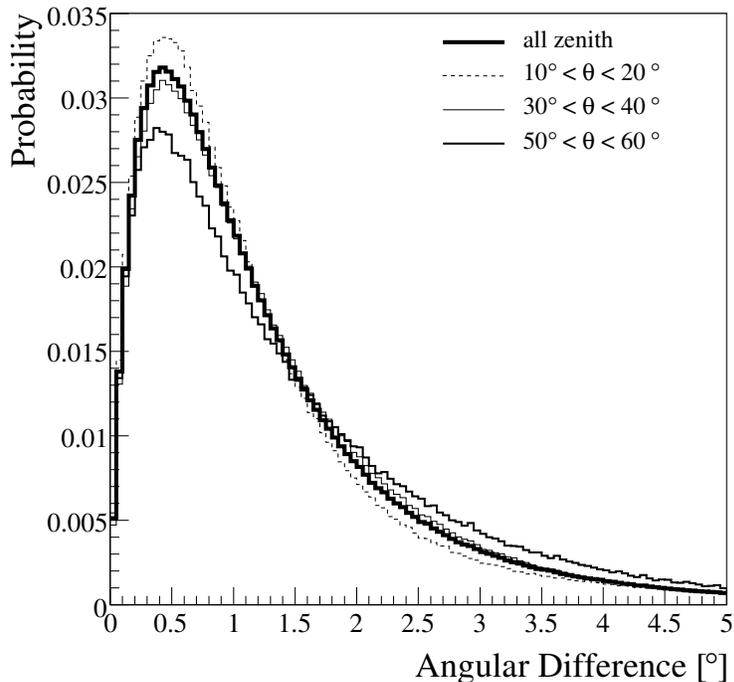
Figure 2: Distributions of the angular difference between the direction of Monte Carlo generated muons at ground level with energies above 30 GeV and the direction of the reconstructed muon track. Three sets for given zenith angle ranges are displayed together with the result for any chosen zenith angle.

been shown [28] through simulations that the best signal/background ratio is obtained for a circular bin of half-angle,

$$\theta_{\text{opt}} = \left(1.58 + 0.7\, e^{-0.88 N^{0.36}}\right) \sigma^\circ \,, \tag{4}$$

where N is the number of background events. The bin with half-angle of θ_{opt} contains nearly 72 % of the signal events if N is sufficiently large ($N > 100$). It has also been shown [28] that for a square bin of same area as a circular bin, the signal to background ratio is only marginally (~ 1.5 %) smaller. Column (a) of Table 1 shows the fraction of events contained within square bins of the specified size for four different muon energy thresholds and any zenith angle between $0°$ and $60°$. The hypothesis is made that muons are at the center of the bin of the reconstructed direction after passing through the molass and the detector.

    If the spread in angle of the muons around the γ-ray direction, due to the pion transverse momentum, is included, the fraction drops by about 10 %, (column (b) of Table 1). A relatively flat differential power law spectrum with a spectral exponent β of -2.0 was assumed for primary γ-rays in the light of published observations of various sources. This yields a slightly harder energy spectrum compared to proton showers whose spectrum is assumed to be steeper with an exponent of -2.7. The detector simulation is based on proton-induced showers. After correcting for this difference, the fraction of events expected to be contained within the square bin is slightly increased as shown in column (c) of Table 1.

6
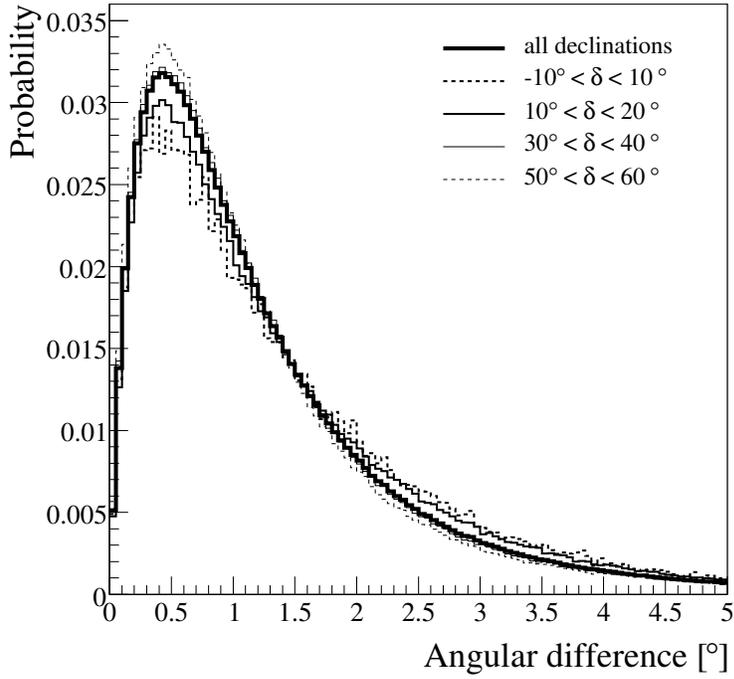
Figure 3: The distribution of the angular difference of muons above 30 GeV entering the matter layers above the detector and the outgoing muons for a set of declination angles integrated over the whole range of accepted zenith angle.

3.3 Search Procedure

To perform the point-source search, the acceptance distribution $N_\mu(\delta, h; E_{\text{cut}})$ in local equatorial coordinates is established. As an example the distribution of the observed muons with energies above 30 GeV for a given data acquisition period is shown in Figure 4. It is obtained from muons inside the detector acceptance and recorded according to the detector's direction-dependent efficiency and is represented by a two-dimensional histogram, $\mathcal{H}^{\mathcal{A}}$, which covers all directions with declination $\delta > \delta_{\text{min}}$. The size p_s of the bins of $\mathcal{H}^{\mathcal{A}}$, called "pixels", is chosen so that

$$l_\alpha = \frac{2\pi}{p_s} \quad \text{and} \quad l_\delta = \frac{\pi/2 - \delta_{\text{min}}}{p_s} \tag{5}$$

are integers. The bin content $N_{i,j}$ corresponds to the number of selected muon tracks seen in the particular pixel (i, j).

The background muon distribution $N_{\text{tot}}^{\text{bkg}}(\delta, \alpha; E_{\text{cut}})$ is determined in equatorial coordinates for the time interval I_t, which can cover either the full period used to fill the histogram $\mathcal{H}^{\mathcal{A}}$, or part of it. Also $N_{\text{tot}}^{\text{bkg}}(\delta, \alpha; E_{\text{cut}})$ is represented by a two dimensional histogram, $\mathcal{H}^{\mathcal{B}}$, which covers all directions of the sky with declination $\delta > \delta_{\text{min}}$ and has the same pixels as $\mathcal{H}^{\mathcal{A}}$. Its bin contents are called $N_{i,j}^{\text{bkg}}$ and correspond to the number of background muon tracks expected in the particular pixel cell. The number of events as a function of the sidereal time $N(t_s)$ is convoluted with the acceptance distribution $N(\delta, h; E_{\text{cut}})$ to get the number of background muons:

$$N_{\text{tot}}^{\text{bkg}}(\delta, \alpha; E_{\text{cut}}) = \int_0^{2\pi} \frac{N(t_s)}{N_{\text{tot}}} \cdot N(\delta, [\alpha - t_s]; E_{\text{cut}}) dt_s , \tag{6}$$

7

Table 1: The optimized angular bin sizes obtained from simulations for different requirements on the muon, for four different muon energy-threshold values. The fraction of all signal events contained in the bin are calculated. Column (a): same conditions as for Figure 2. Column (b): CORSIKA generation with isotropically incident primary gammas with an energy spectrum proportional to E_γ^{-2} and under zenith angles less than 60°, matching the detector acceptance. The effect of the transverse momentum of the secondary hadrons on the angular resolution is included. Column (c): Same as for (b), but after correcting for the difference of the detector simulation for protons and gammas induced events (see text).

Energy cut [GeV]	Bin Size [°]	Fraction of events [%] (a)	Fraction of events [%] (b)	Fraction of events [%] (c)
20	3.0	72.9	64.9	69.7
30	2.4	71.9	65.2	69.6
50	1.5	72.4	65.3	68.8
100	0.9	73.1	67.2	70.9

where N_{tot} is the total number of events.

Figure 5 shows the expected background distribution $N_{\text{tot}}^{\text{bkg}}(\delta, \alpha; E_{\text{cut}})$ for a particular period and $E_{\text{cut}} = 30$ GeV. The pixel size is 1°. This may be compared with the sky map $\mathcal{H}^{\mathcal{C}}$ shown in Figure 6 of the observed $N_{\text{tot}}^{\text{obs}}(\delta, \alpha; E_{\text{cut}})$ distribution for the same period I_t of data taking. The two are very similar. As an example, for a given declination band ($\delta= 40°$ to $45°$) the difference of the two distributions is shown in Figure 7 as a function of α.

A search for a statistically-significant excess in a source bin, relative to the expected background, is made on several time scales, namely, daily, monthly and, for the purpose of comparison with other results, on the full set of selected data (corresponding to an effective live-time of 150.6 days), for 20, 30, 50, 100 GeV. A two-dimensional histogram $H_\mu^{\text{obs}}(\delta, \alpha, E_{\text{cut}})$ for a specified time period is created with bin contents, $N_{i,j}^{\text{obs}}$, which represent the number of observed events in the bin defined by the elements (i, j). In order to assess the significance of a possible excess in the observed distribution the probability P is calculated for finding a number $N^{\text{obs}}(\delta, \alpha, E_{\text{cut}})$ or larger when the number of events expected from the background distribution is $N^{\text{bkg}}(\delta, \alpha, E_{\text{cut}})$ using the Poisson relation:

$$P = 1 - \Sigma_{k=0}^{N^{\text{obs}}} \frac{e^{-N^{\text{bkg}}} N_{\text{bkg}}^k}{k!} \tag{7}$$

The probability P, calculated numerically, is hereafter represented through its base-10 logarithm, $-\log P$.

Knowing the number of background events N^{bkg} and the number of observed events N^{obs}, an upper limit on the number of signal events N^{sig} is determined at the 90 % confidence level (CL) as:
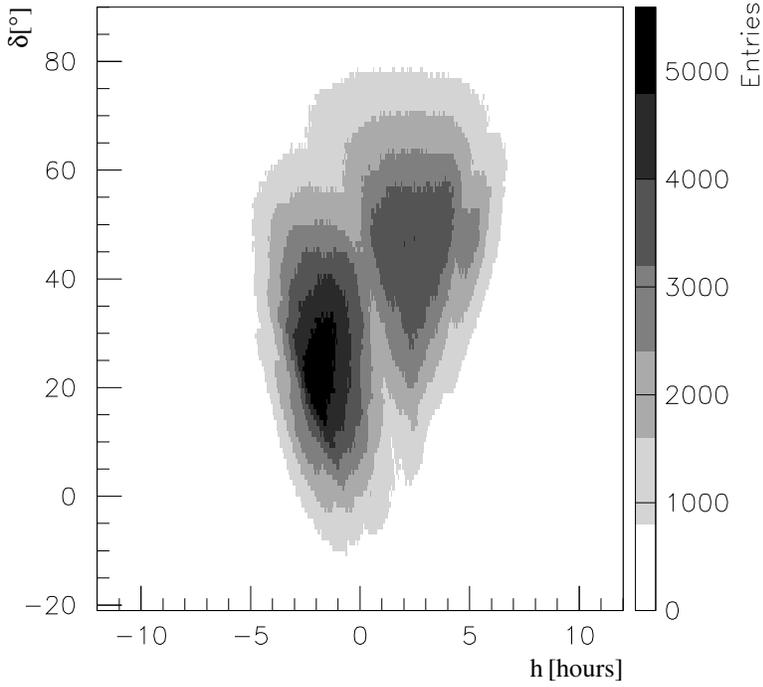
Figure 4: Example, $(\mathcal{H}^{\mathcal{A}})$, of collected events representing the acceptance distribution $N(\delta, \alpha - t_s; E_{\text{cut}})$ in local equatorial coordinates for a given period and a muon energy threshold of 30 GeV. A pixel size of $1°$ is used.

$$\frac{\sum_{n=0}^{N^{\text{obs}}} \text{Poisson}(n|N^{\text{bkg}} + N^{\text{sig}})}{\sum_{n=0}^{N_{\text{obs}}} \text{Poisson}(n|N^{\text{bkg}})} = 0.1 \tag{8}$$

In order to compare with other experimental results, the flux upper limits are estimated for the location of the source to be at the zenith. It is assumed that the zenith-angle dependence of the background and the source flux is similar, such that the signal to background ratio is independent of the direction. The upper limit on the muon flux is then calculated using the relation,

$$\phi_{E_\mu > E_{\text{cut}}}^{\text{ul,vert}} = \frac{1}{F} \frac{N^{\text{sig}}}{N^{\text{bkg}}} \phi_{E_\mu > E_{\text{cut}}}^{\text{bkg,vert}} \Omega_{\text{bin}} X_{\text{m}}, \tag{9}$$

where Ω_{bin} is the solid angle subtended by the search window, and F is the fraction of events which are reconstructed in the square bin for a point source in the direction of the center of the bin. The background vertical flux $\phi_{E_\mu > E_{\text{cut}}}^{\text{bkg,vert}}$ is calculated using the Monte Carlo shower simulation CORSIKA [23] and a normalized muon flux of $0.3 \cdot 10^{-4}$ cm^{-2}s^{-1} at 100 GeV [21]. X_{m} is a correction factor taking into account the momentum resolution of the detector and varies between 0.94 and 1.0. It corresponds to the ratio between the number of selected Monte Carlo events with a generated energy larger than E_{cut} and the number of selected Monte Carlo events with a reconstructed energy larger than E_{cut}. For low energies this correction is negligible.

9
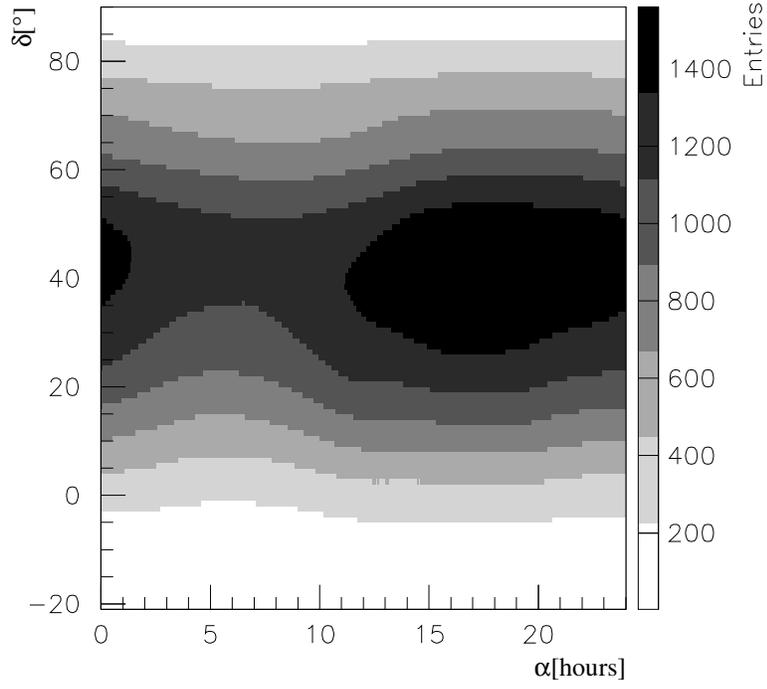
Figure 5: Expected $\mathcal{H}^{\mathcal{B}}$ background distribution $N_{\text{tot}}^{\text{bkg}}(\delta, \alpha; E_{\text{cut}})$ in equatorial coordinates for a given period and a muon energy threshold of 30 GeV. A pixel size of $1°$ is used.
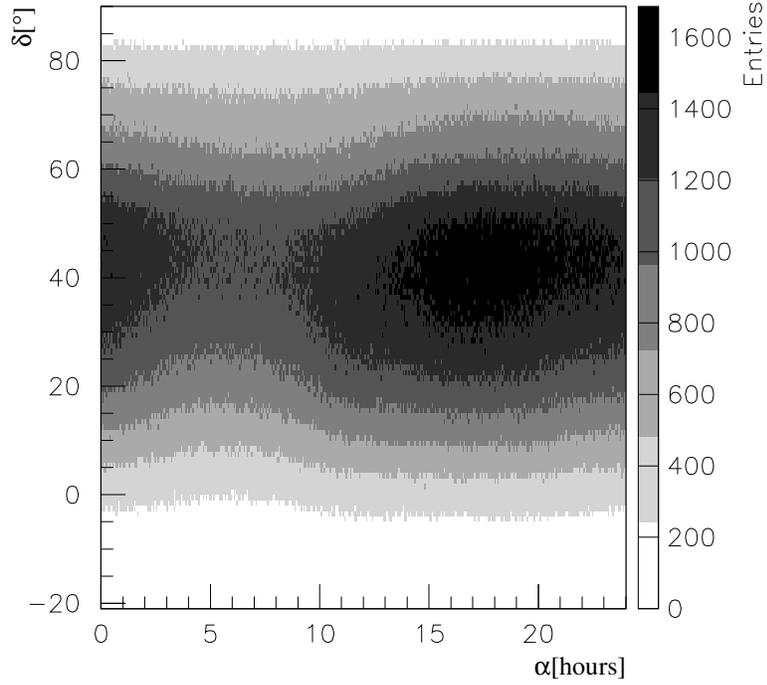
Figure 6: Measured $\mathcal{H}^{\mathcal{C}}$ distribution $N_{\text{tot}}^{\text{obs}}(\delta, \alpha; E_{\text{cut}})$ in equatorial coordinates for a given period and a muon energy threshold of 30 GeV. A pixel size of $1°$ is used.

10
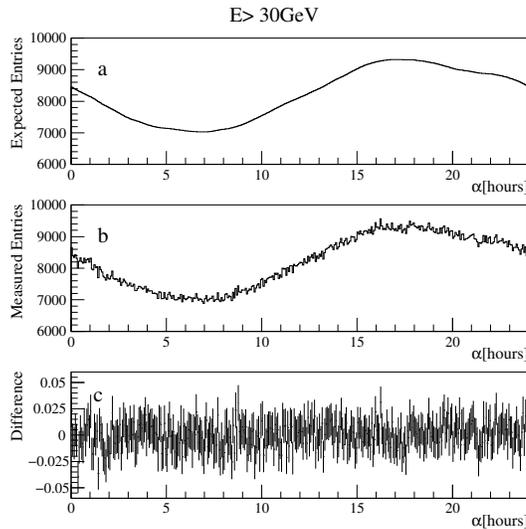
Figure 7: Number of a) expected and b) observed events within a declination band between 40° and 45°. c) Relative difference of a) and b).

4 Search for Signals from Selected Sources

Data are binned for the search for bursts of muon events from 10 selected sources listed in Table 2, with a declination width (Δ_δ) using the values given in the second column of Table 1. In order to have a window of approximately the same width in declination and right ascension, the width of the right ascension bin is taken as $\Delta_\delta / \cos \delta$.

As emphasized earlier, the main advantage of muon telescopes lies in the daily monitoring of all sources located within the accessible declination band, and the potential for detection of a large flare from any of these sources. The search for intense flares is carried out by looking for large excesses on shorter time scales, for example, one day. Figure 8 shows the distributions of the $-\log P$ values combined for all the 10 sources for a threshold value of 20 GeV. The dashed line shows the expectation for the Poisson distribution. Data for each day and for each of the 10 sources contribute one entry to the distribution. No significant excess is observed. A similar conclusion is reached for the other three energy cuts.

Instead of listing upper flux limits for each day analyzed (which vary due to detector inefficiencies and source positions), median upper muon flux limits at 90% CL (Confidence Level) for data collected during one day with smooth running conditions are given in Table 2. The effective live-time involved for these results amounts to 150.6 days distributed over the full data aquisition time July to November 1999 and April to November 2000.

In table 3 a comparison is made between L3+C flux limits obtained from the 1999 and 2000 periods and the MACRO data [20] (2000) collected between February 1989 and December 2000. A comparison with results of other underground experiments [29] can only be performed with published data for steady or modulated emissions. In Figure 9 muon-flux limits and two values are compiled for Cyg X-3 as an illustration. L3+C gives the only "steady" muon flux limits for energy thresholds above 20, 30, 50 and 100 GeV. The extrapolation of the four flux limits to higher energies lies below all other limits of modulated signals, except the one measured by MACRO.
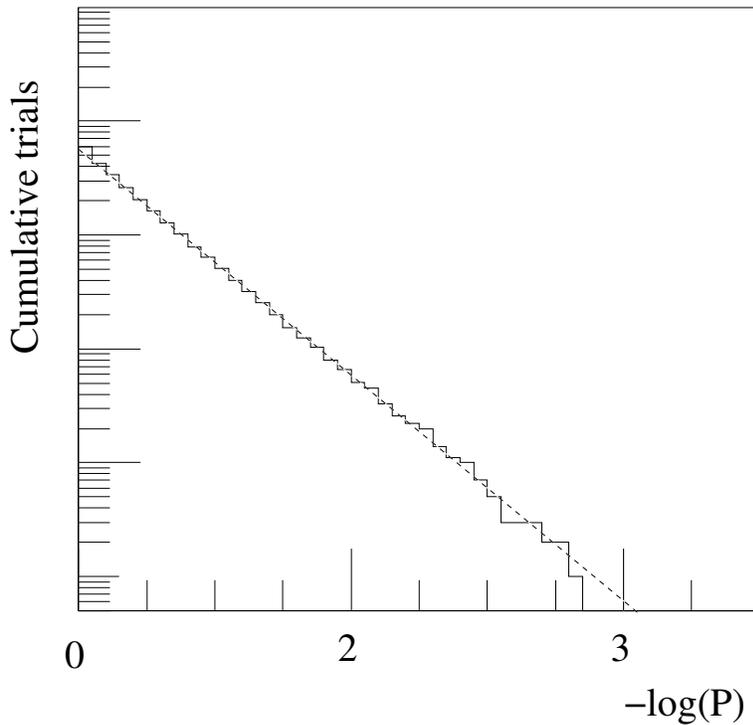
Figure 8: Cumulative distribution of $-\log P$ for daily analysis of the 10 selected point sources. There is one entry per source and per analyzed one day interval. The muon threshold energy is 20 GeV. The dashed line represents the expected distribution.

5 Sky Survey

A survey of the sky is performed over different time scales: 1 day, a few weeks, months. This search is performed for four different muon energy thresholds, namely 20, 30, 50 and 100 GeV. The Poisson probability P to find a number of events larger than or equal to N^{obs}, when the number of background events is N^{bkg}, is calculated for each bin.

As discussed above, the size of the angular bin is optimized through simulations and grouping pixels such that $\sim 70\%$ of the signal events are contained within the bin.

Figure 10 shows the cumulative distributions for $-\log P$ for all one-day periods and for the four different muon energy thresholds. No significant excess is seen. Similar plots are obtained for each data taking period. Again for this survey the typical upper limits on the flux of muons originating from any direction of the northern hemisphere for data collected during one day with smooth running conditions are listed in Table 4 for one day lasting flares. Also given are the limits for constant emission during the full data aquisition period, allowing again for a comparison with other underground experiments.

Table 2: Median upper muon flux limits with 90 % CL for selected sources, and for data collected during one day with smooth running conditions.

Source	$E_\mu > 20\text{GeV}$ $3° \times 3°$ [cm^{-2}s^{-1}]	$E_\mu > 30\text{GeV}$ $2.4° \times 2.4°$ [cm^{-2}s^{-1}]	$E_\mu > 50\text{GeV}$ $1.5° \times 1.5°$ [cm^{-2}s^{-1}]	$E_\mu > 100\text{GeV}$ $0.9° \times 0.9°$ [cm^{-2}s^{-1}]
Mkn 421	$3.6 \cdot 10^{-8}$	$1.5 \cdot 10^{-8}$	$5.2 \cdot 10^{-9}$	$1.3 \cdot 10^{-9}$
Mkn 501	$3.6 \cdot 10^{-8}$	$1.5 \cdot 10^{-8}$	$5.2 \cdot 10^{-9}$	$1.3 \cdot 10^{-9}$
3C 273	$8.1 \cdot 10^{-8}$	$3.5 \cdot 10^{-8}$	$11. \cdot 10^{-9}$	$3.1 \cdot 10^{-9}$
Crab nebula	$4.7 \cdot 10^{-8}$	$2.0 \cdot 10^{-8}$	$6.6 \cdot 10^{-9}$	$1.6 \cdot 10^{-9}$
Cyg X-1	$3.9 \cdot 10^{-8}$	$1.6 \cdot 10^{-8}$	$5.6 \cdot 10^{-9}$	$1.4 \cdot 10^{-9}$
Cyg X-3	$3.8 \cdot 10^{-8}$	$1.5 \cdot 10^{-8}$	$5.3 \cdot 10^{-9}$	$1.3 \cdot 10^{-9}$
Her X-1	$4.0 \cdot 10^{-8}$	$1.7 \cdot 10^{-8}$	$5.7 \cdot 10^{-9}$	$1.5 \cdot 10^{-9}$
Geminga	$4.9 \cdot 10^{-8}$	$2.1 \cdot 10^{-8}$	$7.4 \cdot 10^{-9}$	$1.8 \cdot 10^{-9}$
1ES 1426+428	$3.7 \cdot 10^{-8}$	$1.5 \cdot 10^{-8}$	$5.4 \cdot 10^{-9}$	$1.3 \cdot 10^{-9}$
1ES 2344+514	$3.2 \cdot 10^{-8}$	$1.4 \cdot 10^{-8}$	$5.0 \cdot 10^{-9}$	$1.4 \cdot 10^{-9}$

Table 3: Upper muon flux limits (90 % CL) for selected sources obtained from the full data aquisition period and compared to MACRO data (1989-2000).

Source	L3+C $E_\mu > 20\text{GeV}$ $3° \times 3°$ [cm^{-2}s^{-1}]	L3+C $E_\mu > 100\text{GeV}$ $0.9° \times 0.9°$ [cm^{-2}s^{-1}]	MACRO $E_\mu > 1000\text{GeV}$ Half cone of 1° [cm^{-2}s^{-1}]
Mkn 421	$1.7 \cdot 10^{-9}$	$7.4 \cdot 10^{-11}$	$1.6 \cdot 10^{-13}$
Mkn 501	$2.0 \cdot 10^{-9}$	$7.3 \cdot 10^{-11}$	$3.4 \cdot 10^{-13}$
3C 273	$4.3 \cdot 10^{-9}$	$3.1 \cdot 10^{-10}$	$3.1 \cdot 10^{-13}$
Crab nebula	$6.2 \cdot 10^{-9}$	$1.2 \cdot 10^{-10}$	$3.6 \cdot 10^{-13}$
Cyg X-1	$2.8 \cdot 10^{-9}$	$9.8 \cdot 10^{-11}$	
Cyg X-3	$3.1 \cdot 10^{-9}$	$8.6 \cdot 10^{-11}$	$2.4 \cdot 10^{-13}$
Her X-1	$3.3 \cdot 10^{-9}$	$1.8 \cdot 10^{-10}$	$2.8 \cdot 10^{-13}$
Geminga	$3.4 \cdot 10^{-9}$	$1.2 \cdot 10^{-10}$	$3.1 \cdot 10^{-13}$
1ES 1426+428	$2.8 \cdot 10^{-9}$	$1.7 \cdot 10^{-10}$	
1ES 2344+514	$1.5 \cdot 10^{-9}$	$1.5 \cdot 10^{-10}$	
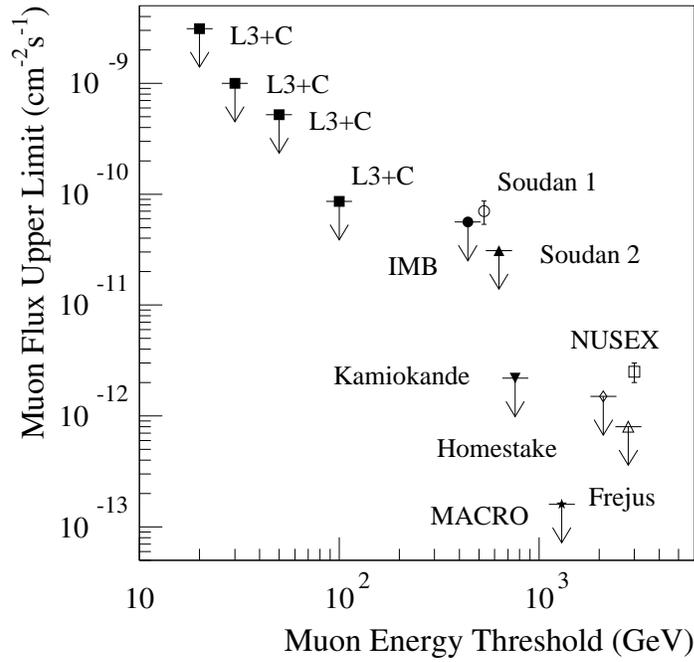
Figure 9: Comparison of muon-flux upper limits and measurements obtained by different experiments searching for modulated signals from Cyg X-3. The L3+C values are from a non-modulated signal search.

Table 4: Range of typical upper muon flux limits from any direction in the northern hemisphere (see text). The limits depend on the coordinates of the virtual source position.

Energy [GeV]	One day periods (90 % CL) [cm^{-2}s^{-1}]	Full period (90 % CL) [cm^{-2}s^{-1}]
20	$1.2 \cdot 10^{-8} - 2.4 \cdot 10^{-7}$	$1.0 \cdot 10^{-9} - 20 \cdot 10^{-9}$
30	$2.4 \cdot 10^{-9} - 6.1 \cdot 10^{-8}$	$0.2 \cdot 10^{-9} - 5 \cdot 10^{-9}$
50	$1.2 \cdot 10^{-9} - 2.4 \cdot 10^{-8}$	$1.0 \cdot 10^{-10} - 20 \cdot 10^{-10}$
100	$2.4 \cdot 10^{-10} - 6,1 \cdot 10^{-9}$	$0.2 \cdot 10^{-10} - 5 \cdot 10^{-10}$

6 Upper γ-ray flux limits

Results and discussion in the preceding sections have shown that 'muon astronomy' at energies above 20 GeV, using the L3 muon telescope-cum-spectrometer located underground at a shallow depth with excellent angular and momentum resolution, has provided interesting upper limits on the muon flux from potential flaring γ-ray sources. In order to relate the upper limit on the muon flux to an upper limit on the γ-ray flux, Monte Carlo simulations have been

14

Analysis on periods of 1 day
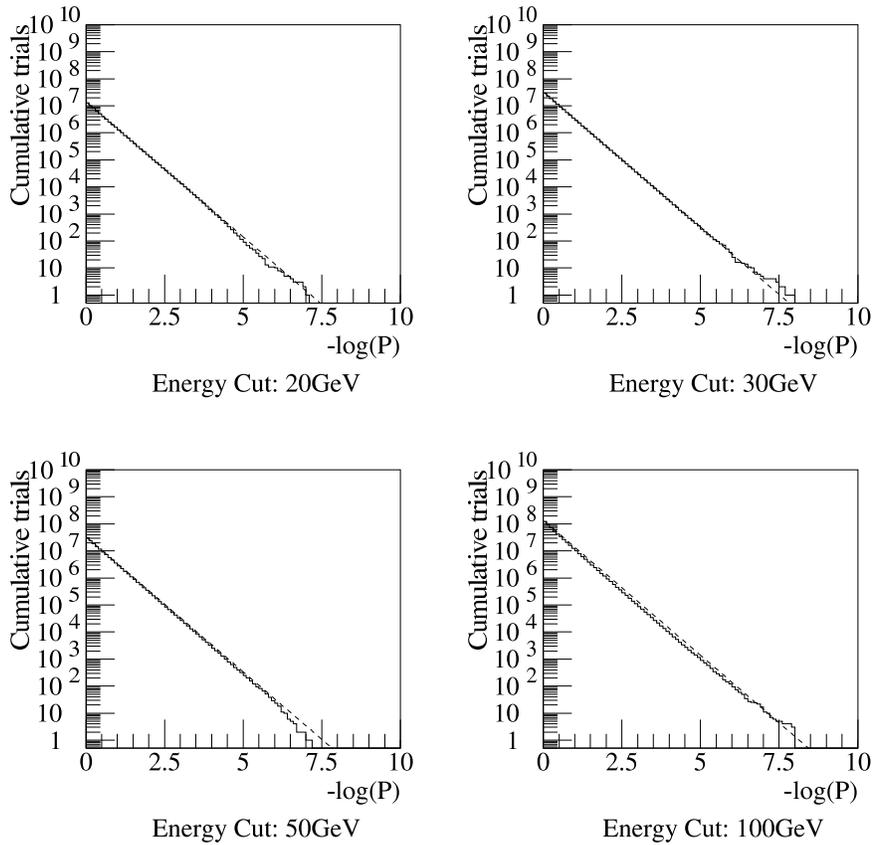
Figure 10: Cumulative distributions of $-\log P$ for different muon threshold-energies. There is one entry for each direction and for each analyzed one day period.

performed with CORSIKA [23]. For this purpose, muon detection-efficiency for muons above 20 GeV observed with the L3+C spectrometer has been computed for primary γ-rays for different energies and arrival angles. These simulations show that the muon detection-efficiency is a linear function of the primary γ-ray energy (see Figure 11) and practically no zenith angle dependence has been observed for $\theta_{zenith} < 45°$. These calculations have been repeated assuming a relatively flat energy spectrum for a primary γ-ray flux with a differential power-law spectral index of -2.0 and a cut-off at 100 TeV. Note that a steeper spectrum for primary γ-rays is expected to yield correspondingly lower number of muons. $4 \cdot 10^6$ gamma showers $(= N_\gamma)$ generated for vertically incident primaries with energies above 50 GeV have been analyzed to get the number of muons produced $(= N_\mu)$ with different energy thresholds E_μ^{cut} : 20, 30, 50 and 100 GeV. Table 5 presents the results of these simulations.

Using the relation between the muon detection-efficiency $\eta(E_\gamma)$ $(= N_\mu/N_\gamma)$, and the energy E_γ of the primary γ-ray shown in Figure 11, the observable muon flux, $\phi_{E_\mu > E_\mu^{\text{cut}}}^{\mu,\text{vert}}$, can be calculated from the primary γ-ray flux $\phi_\gamma(E_\gamma)$ as follows:

$$\phi_{E_\mu > E_\mu^{\text{cut}}}^{\mu,\text{vert}} = \int_{E_\gamma = E_\mu^{\text{cut}}}^{\infty} \phi_\gamma(E_\gamma) \times \eta_\gamma(E_\gamma) \, dE_\gamma \,, \tag{10}$$

15

that is,

$$\phi^{\mu,\text{vert}}_{E_\mu > E^{\text{cut}}_\mu} = \int_{E_\gamma = E^{\text{cut}}_\mu}^{\infty} \phi_\gamma(E_\gamma) \times 1.15 \cdot 10^{-5} \cdot E_\gamma \ dE_\gamma \qquad (11)$$

A comparison of the integrated yield of muons of energy > 20 GeV given in Table 5 for γ-rays of energy > 50 GeV with the values of the yield shown in Figure 11 for various discrete energies shows that the effective average energy of primary γ-rays is ~ 750 GeV for the set of assumptions about the spectrum mentioned above. The observable muon flux is therefore $\sim 8 \cdot 10^{-3}$ of the primary γ-ray flux.
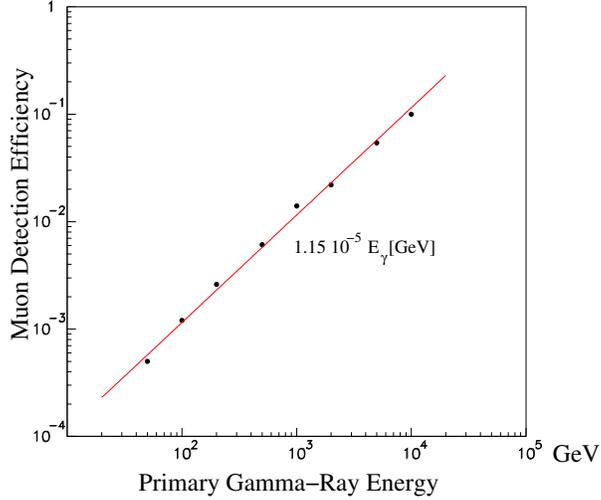
Figure 11: Muon detection-efficiency for muons above 20 GeV observed with the L3+C spectrometer as a function of the primary energy for vertically incident gamma rays.

Table 5: Results of the CORSIKA simulation for $4 \cdot 10^6$ vertically incident gamma showers with primary energies above 50 GeV and a power energy spectrum with index -2.0. The number of muons produced, as well as the muon yield is listed as a function of the muon energy-threshold energy.

Muon threshold Energy [GeV]	Number of muons produced	Muon yield
20	31157	$7.8 \cdot 10^{-3}$
30	18426	$4.6 \cdot 10^{-3}$
50	8739	$2.2 \cdot 10^{-3}$
100	2929	$7.4 \cdot 10^{-4}$
1000	37	$9.3 \cdot 10^{-6}$

Using the results from the simulations shown in the Table 5, the upper limit on the γ-ray Flux, $\phi^{\text{ul}}_{E_\gamma > 50\,GeV}$, has been estimated from the observed upper limit on the muon flux, $\phi^{\text{ul,vert}}_{E_\mu > E^{\text{cut}}_\mu}$ through the simple relation:

$$\phi^{\text{ul}}_{E_\gamma > 50\,GeV} \;=\; \phi^{\text{ul,vert}}_{E_\mu > E^{\text{cut}}_\mu} \times N_\gamma / N_\mu. \tag{12}$$

The resulting upper limits on the γ-ray flux values with 90 % CL obtained from observations on muons with energies above 20 GeV for selected sources, ranges between $4 \cdot 10^{-6}$ and $1 \cdot 10^{-5}\,\text{cm}^{-2}\text{s}^{-1}$ in the case of flares lasting only one day, and between $2 \cdot 10^{-7}$ and $8 \cdot 10^{-7}\,\text{cm}^{-2}\text{s}^{-1}$ in the case of steady signals. The sky survey gives upper flux limits of $3 \cdot 10^{-5}$ and $2.5 \cdot 10^{-6}\,\text{cm}^{-2}\text{s}^{-1}$ for the two cases respectively.

A comparison of these upper limits on the γ-ray flux with the flux values observed [13] using the Cherenkov technique for some of the sources, for example, the AGNs Mkn 421 and Mkn 501, shows that the observations with high energy muons can detect only very intense short duration bursts. As was pointed out earlier, the very small efficiency is a result of not only the very small probability for the production of muons by primary γ-rays, but also the relatively much smaller effective detection area of the muon spectrometer as compared to the very large area over which the Cherenkov photons, produced near the shower maximum in the upper atmosphere, are spread. The area of the Cherenkov radiation pool, ~ 100 m radius around the projected core position of the shower on the ground, is almost 300 times the effective area of the muon spectrometer ($\sim 100 m^2$). In this sense, the observations on high energy muons with a large area precision spectrometer are similar to the observations with satellite-borne detectors, for example, the EGRET detector on the CGRO [30], as their effective γ-ray detection area is also smaller than the physical area of the detector. Unfortunately, the effective detection area of satellite-borne detectors can not be increased arbitrarily due to practical limitations. They are relatively unsuitable for observations on the high energy tail of the energy spectrum of γ-ray sources which carries very significant information on the physical process generating the γ-ray flux in the source.

However, the real value of the observations on high energy muons for γ-ray astronomy lies in its capability of monitoring a large part of the sky with high efficiency on daily basis, independent of the local atmospheric weather conditions. The two major features of the Cherenkov technique, small field of view and small observational efficiency due to frequent presence of the moon and clouds in the sky, make this very powerful and highly successful technique relatively unsuitable for monitoring vast areas of the sky for as yet unknown high energy astrophysical sources which may be flaring up in the high energy γ-ray part of the energy spectrum. The two techniques, the high energy muon and the Cherenkov radiation, may therefore be considered complementary to each other. A small region of the sky observed to be showing a flaring source in high energy muons during the round-the-clock monitoring, can be studied immediately afterwards in much greater detail and with high precision with imaging Cherenkov telescopes around the world.

7   Conclusions

The high-resolution muon spectrometer of the L3+C experiment has been used for a search for cosmic sources of very high energy γ-ray emission during 312 days spread over the periods, July-November 1999 and April-November 2000. It has been shown that observations with a

precision muon spectrometer offers the possibility to search for large flares on a day-to-day basis, unaffected by atmospheric conditions unlike Cherenkov radiation telescopes.

Of the ten interesting sources studied with data from the L3+C spectrometer, no flaring signal has been detected over the relatively short observation period and 90 %CL upper limits have been placed on the flux of muons of energy $> 20, 30, 50$ and 100 GeV. Also, sky surveys for large flares from yet unknown sources have not revealed any interesting episode at different time scales. For an assumed energy spectrum of primary gamma rays upper flux limits have been derived corresponding to a 20 GeV muon threshold.

Acknowledgments

References

[1] P.L. Bierman *et al.*, *Astron. Astrophys.* **369** (2000) 269.

[2] CANGAROO collab.: M. Mori, Proc. Int'l. Symposium on High Energy Gamma-Ray Astronomy, Heidelberg, Germany, 26−30 June 2000.

[3] HESS collab.: J.A. Hinton, *New Astron. Rev.* **48** (2004) 331.

[4] MAGIC collab.: E. Lorenz, *New Astron. Rev.* **48** (2004) 339.

[5] VERITAS collab.: T.C. Weekes *et al.*, proposal, Smithsonian Astrophysical Observatory, November 1996.

[6] HEGRA collab.: F. Aharonian *et al.*, *Astron. Astrophys.* **327** (1997) L5;
HEGRA collab.: K. Okumura *et al.*, *Astrophys. J. Lett.* **579** (2002) L9-L12;
HEGRA collab.: T. Antoni *et al.*, *Astrophys. J.* **608** (2004) 865.

[7] MILAGRO collab.: R. Atkins *et al.*, *Astrophys. J. Lett.* **533** (2000) L119;
MILAGRO collab.: R. Atkins *et al.*, *Astrophys. J. Lett.* **525** (1999) L25.

[8] T. Stanev, *Phys. Rev.* **D33** (1986) 2740;
M. Drees and F. Halzen, *Phys. Rev.* **D39** (1989) 1310;
F. Halzen *et al.*, *Phys. Rev.* **D55** (1997) 4475;
N. Gupta and D.B. Bhattacharya, *Phys. Lett.* **B514** (2001) 321;
L.M. Boone *et al.*, *Astrophys. J. Lett.* **579** (2002) L5;
F. Krennrich *et al.*, *Astrophys. J.* **511** (1999) 149.

[9] Whipple collab.: M. Schubnell *et al.*, VIIth Int'l. Symposium on Very High Energy Cosmic Ray Interactions, AIP Conf. Proc. **276**, (1993) 185;
Whipple collab.: F. Krennrich *et al.*, Proc. XXVIth ICRC, Salt Lake City, 1999, and Proceedings of the XXVth ICRC, Durban 1997;
Whipple collab.: J.A. Gaidos *et al.*, Nature **383** (1996) 26;

HEGRA collab.: F.A. Aharonian *et al.*, *Astron. Astrophys.* **410** (2003) 813;
HEGRA collab.: F.A. Aharonian *et al.*, *Astron. Astrophys.* **349** (1999) 11;
HEGRA collab.: K. Okumura *et al.*, *Astrophys. J. Lett.* **579** (2002) L9-L12.

[10] SOUDAN I collab.: M.L. Marshak *et al.*, *Phys. Rev. Lett.* **54** (1985) 2079;
SOUDAN I collab.: M.L. Marshak *et al.*, *Phys. Rev. Lett.* **55** (1985) 1965.

[11] NUSEX collab.: G. Battistoni *et al.*, *Phys. Lett.* **B155** (1985) 465.

[12] Kiel collab.: A. Alkofer *et al.*, Proc. XVIIIth ICRC, Bangalore, 1983;
Cygnus collab.: B.L. Dingus *et al.*, *Phys. Rev. Lett.* **60** (1988) 1785.

[13] R.A. Ong, *Phys. Rep.* **305** (1998) 93.

[14] CASA-MIA collab.: A. Barione *et al.*, *Phys. Rev.* **D 55** (1997) 1714.

[15] KASCADE collab.: T. Antoni *et al.*, Astrophys. J. **608** (2004) 865.

[16] SOUDAN II collab.: M. Thomson *et al.*, *Phys. Lett.* **B269** (1991) 220.

[17] S. C. Tonwar *Bull. Ind. Astron. Soc. India* **30** (2002) 147.

[18] L3 collab.: B. Adeva *et al.*, *Nucl. Instr. Meth.* **A 289** (1990) 35.

[19] L3+C collab.: O. Adriani *et al.*, *Nucl. Inst. Meth.* **A 488** (2002) 209;
L3 collab.: P.Achard *et al.*, *Phys. Lett.* **B 598** (2004) 15.

[20] MACRO collab.: M. Ambrosio *et al.*, *Astropart. Phys.* **18** (2003) 615;
MACRO collab.: S.P. Ahlen *et al.*, *Astrophys. J.* **412** (1993) 301;
MACRO collab.: C. Satriano *et al.*, Proc. XXVI ICRC, Salt Lake City, 1999.

[21] R. Ramelli, "Search for Cosmic Ray Point Sources and Anisotropy Measurement with the L3+C Experiment", PhD thesis No. 14683, ETH-Zürich, 2002.

[22] M. Unger, "Measurement of the momentum spectrum of atmospheric muons with the L3 detector", PhD thesis, Humboldt-University, Berlin, 2003.

[23] D. Heck *et al.*, CORSIKA, Version 5.62, Technical report, FZKA 6019, Forschungszentrum Karlsruhe (1998).

[24] N.N. Kalmykov, *et al.*, *Yad. Fiz.* **56** (1993) 105;
N.N. Kalmykov, *et al.*, *Nucl.Phys.Proc.Suppl.* **B 52** (1997) 17

[25] GEANT Version 3.15; R. Brun *et al.*, preprint DD/EE/84-1 (1984), revised 1987.

[26] L3 collab.: P. Achard *et al.*, *Astropart. Phys.* **23** (2005) 411.

[27] Y.P. Xu, "Search for TeV-Antiprotons in Space from the Shadowing of Cosmic Rays by the Moon with the L3+C Detector", thesis 2005, ETH Zürich.

[28] D.E. Alexandreas *et al.*, *Nucl. Instr. Meth.* **A 328** (1993) 570.

[29] IMB collab.: R. Bionta *et al.*, *Phys. Rev.* **D36** (1987) 30;
SOUDAN 1 collab.: M.L. Marshak *et al.*, *Phys. Rev. Lett.* **54** (1985) 2079;
SOUDAN 2 collab.: J.A. Kochocki *et al.*, *Phys. Rev.* **D42** (1990) 2967;
Kamiokande collab.: Y. Oyama *et al.*, *Phys. Rev. Lett.* **56** (1986) 991;
MACRO collab.: M. Ambrosio *et al.*, *Astropart. Phys.* **18** (2003) 615;
Homestake collab.: cited in *Astropart. Phys.* **18** (2003) 615;
Fréjus collab.: Ch. Berger *et al.*, *Phys. Lett.* **B171** (1986) 118;
NUSEX collab.: G. Battistoni *et al.*, *Phys. Lett.* **B155** (1985) 465.

[30] E.B. Hughes, *et al.*, *IEEE Trans. Nucl. Sci.* **NS-27** (1980) 364;
EGRET collab., R.C. Hartman, *et al.*, *Astrophys. J. Suppl.* **Ser 123** (1999) 79.

The L3 Collaboration:

P.Achard,[22] O.Adriani,[19] M.Aguilar-Benitez,[27] M.van den Akker,[33] J.Alcaraz,[27] G.Alemanni,[25] J.Allaby,[20] A.Aloisio,[31] M.G.Alviggi,[31] H.Anderhub,[53] V.P.Andreev,[6,37] F.Anselmo,[10] A.Arefiev,[30] T.Azemoon,[3] T.Aziz,[11] P.Bagnaia,[42] A.Bajo,[27] G.Baksay,[28] L.Baksay,[28] J.Bähr,[52] S.V.Baldew,[2] S.Banerjee,[11] Sw.Banerjee,[4] A.Barczyk,[53,51] R.Barillère,[20] P.Bartalini,[25] M.Basile,[10] N.Batalova,[50] R.Battiston,[36] A.Bay,[25] F.Becattini,[19] U.Becker,[15] F.Behner,[53] L.Bellucci,[19] R.Berbeco,[3] J.Berdugo,[27] P.Berges,[15] B.Bertucci,[36] B.L.Betev,[53] M.Biasini,[36] M.Biglietti,[31] A.Biland,[53] J.J.Blaising,[4] S.C.Blyth,[38] G.J.Bobbink,[2] A.Böhm,[1] L.Boldizsar,[14] B.Borgia,[42] S.Bottai,[19] D.Bourilkov,[53] M.Bourquin,[22] S.Braccini,[22] J.G.Branson,[44] F.Brochu,[4] J.D.Burger,[15] W.J.Burger,[36] X.D.Cai,[15] M.Capell,[15] G.Cara Romeo,[10] G.Carlino,[31] A.Cartacci,[19] J.Casaus,[27] F.Cavallari,[42] N.Cavallo,[39] C.Cecchi,[36] M.Cerrada,[27] M.Chamizo,[22] Y.H.Chang,[48] M.Chemarin,[26] A.Chen,[48] G.Chen,[7] G.M.Chen,[7] H.F.Chen,[24] H.S.Chen,[7] T.Chiarusi,[19] G.Chiefari,[31] L.Cifarelli,[43] F.Cindolo,[10] I.Clare,[15] R.Clare,[41] G.Coignet,[4] N.Colino,[27] S.Costantini,[42] B.de la Cruz,[27] S.Cucciarelli,[36] R.de Asmundis,[31] P.Déglon,[22] J.Debreczeni,[14] A.Degré,[4] K.Dehmelt,[28] K.Deiters,[51] D.della Volpe,[31] E.Delmeire,[22] P.Denes,[40] F.DeNotaristefani,[42] A.De Salvo,[53] M.Diemoz,[42] M.Dierckxsens,[2] L.K.Ding,[7] C.Dionisi,[42] M.Dittmar,[53] A.Doria,[31] M.T.Dova,[12,♯] D.Duchesneau,[4] M.Duda,[1] I.Duran,[45] B.Echenard,[22] A.Eline,[20] A.El Hage,[1] H.El Mamouni,[26] A.Engler,[38] F.J.Eppling,[15] P.Extermann,[22] G.Faber,[53] M.A.Falagan,[27] S.Falciano,[42] A.Favara,[35] J.Fay,[26] O.Fedin,[37] M.Felcini,[53] T.Ferguson,[38] H.Fesefeldt,[1] E.Fiandrini,[36] J.H.Field,[22] F.Filthaut,[33] P.H.Fisher,[15] W.Fisher,[40] I.Fisk,[44] G.Forconi,[15] K.Freudenreich,[53] C.Furetta,[29] Yu.Galaktionov,[30,15] S.N.Ganguli,[11] P.Garcia-Abia,[27] M.Gataullin,[35] S.Gentile,[42] S.Giagu,[42] Z.F.Gong,[24] H.J.Grabosch,[52] G.Grenier,[26] O.Grimm,[53] H.Groenstege,[2] M.W.Gruenewald,[18] M.Guida,[43] Y.N.Guo,[7] S.K.Gupta,[11] V.K.Gupta,[40] A.Gurtu,[11] L.J.Gutay,[50] D.Haas,[5] Ch.Haller,[53] D.Hatzifotiadou,[10] Y.Hayashi,[34] Z.X.He,[8] T.Hebbeker,[1] A.Hervé,[20] J.Hirschfelder,[38] H.Hofer,[53] H.Hofer,jun.,[53] M.Hohlmann,[28] G.Holzner,[53] S.R.Hou,[48] A.X.Huo,[7] N.Ito,[34] B.N.Jin,[7] P.Jindal,[16] C.L.Jing,[7] L.W.Jones,[3] P.de Jong,[2] I.Josa-Mutuberría,[27] V.Kantserov,[52,⊙] M.Kaur,[16] S.Kawakami,[34] M.N.Kienzle-Focacci,[22] J.K.Kim,[47] J.Kirkby,[20] W.Kittel,[33] A.Klimentov,[15,30] A.C.König,[33] E.Kok,[2] A.Korn,[15] M.Kopal,[50] V.Koutsenko,[15,30] M.Kräber,[53] H.H.Kuang,[7] R.W.Kraemer,[38] A.Krüger,[52] J.Kuijpers,[33] A.Kunin,[15] P.Ladron de Guevara,[27] I.Laktineh,[26] G.Landi,[19] M.Lebeau,[20] A.Lebedev,[15] P.Lebrun,[26] P.Lecomte,[53] P.Lecoq,[20] P.Le Coultre,[53,⊕] J.M.Le Goff,[20] Y.Lei,[7] H.Leich,[52] R.Leiste,[52] M.Levtchenko,[29] P.Levtchenko,[37] C.Li,[24] L.Li,[7] Z.C.Li,[7] S.Likhoded,[52] C.H.Lin,[48] W.T.Lin,[48] F.L.Linde,[2] L.Lista,[31] Z.A.Liu,[7] W.Lohmann,[52] E.Longo,[42] Y.S.Lu,[7] C.Luci,[42] L.Luminari,[42] W.Lustermann,[53] W.G.Ma,[24] X.H.Ma,[7] Y.Q.Ma,[7] L.Malgeri,[22] A.Malinin,[30] C.Maña,[27] J.Mans,[40] J.P.Martin,[26] F.Marzano,[42] K.Mazumdar,[11] R.R.McNeil,[6] S.Mele,[20,31] X.W.Meng,[7] L.Merola,[31] M.Meschini,[19] W.J.Metzger,[33] A.Mihul,[13] A.van Mil,[33] H.Milcent,[20] G.Mirabelli,[42] J.Mnich,[1] G.B.Mohanty,[11] B.Monteleoni,[19,†] G.S.Muanza,[26] A.J.M.Muijs,[2] B.Musicar,[44] M.Musy,[42] S.Nagy,[17] R.Nahnhauer,[52] V.A.Naumov,[19,◊] S.Natale,[22] M.Napolitano,[31] F.Nessi-Tedaldi,[53] H.Newman,[35] A.Nisati,[42] T.Novak,[33] H.Nowak,[52] R.Ofierzynski,[53] G.Organtini,[42] I.Pal,[50] C.Palomares,[27] P.Paolucci,[31] R.Paramatti,[42] J.-F.Parriaud,[26] G.Passaleva,[19] S.Patricelli,[31] T.Paul,[12] M.Pauluzzi,[36] C.Paus,[15] F.Pauss,[53] M.Pedace,[42] S.Pensotti,[29] D.Perret-Gallix,[4] B.Petersen,[33] D.Piccolo,[31] F.Pierella,[10] M.Pieri,[19] M.Pioppi,[36] P.A.Piroué,[40] E.Pistolesi,[29] V.Plyaskin,[30] M.Pohl,[22] V.Pojidaev,[19] J.Pothier,[20] D.Prokofiev,[37] J.Quartieri,[43] C.R.Qing,[8] G.Rahal-Callot,[53] M.A.Rahaman,[11] P.Raics,[17] N.Raja,[11] R.Ramelli,[53] P.G.Rancoita,[29] R.Ranieri,[19] A.Raspereza,[52] K.C.Ravindran,[11] P.Razis,[32] D.Ren,[53] M.Rescigno,[42] S.Reucroft,[12] P.Rewiersma,[2,†] S.Riemann,[52] K.Riles,[3] B.P.Roe,[3] A.Rojkov,[53,33,19] L.Romero,[27] A.Rosca,[52] C.Rosemann,[1] C.Rosenbleck,[1] S.Rosier-Lees,[4] S.Roth,[1] J.A.Rubio,[20] G.Ruggiero,[19] H.Rykaczewski,[53] R.Saidi,[9] A.Sakharov,[53] S.Saremi,[6] S.Sarkar,[42] J.Salicio,[20] E.Sanchez,[27] C.Schäfer,[20] V.Schegelsky,[37] V.Schmitt,[9] B.Schoeneich,[52] H.Schopper,[23] D.J.Schotanus,[33] C.Sciacca,[31] L.Servoli,[36] C.Q.Shen,[7] S.Shevchenko,[35] N.Shivarov,[46] V.Shoutko,[15] E.Shumilov,[30] A.Shvorob,[35] D.Son,[47] C.Souga,[26] P.Spillantini,[19] M.Steuer,[15] D.P.Stickland,[40] B.Stoyanov,[46] A.Straessner,[22] K.Sudhakar,[11] H.Sulanke,[52] G.Sultanov,[46] L.Z.Sun,[24] S.Sushkov,[1] H.Suter,[53] J.D.Swain,[12] Z.Szillasi,[28,¶] X.W.Tang,[7] P.Tarjan,[17] L.Tauscher,[5] L.Taylor,[12] B.Tellili,[26] D.Teyssier,[26] C.Timmermans,[33] Samuel C.C.Ting,[15] S.M.Ting,[15] S.C.Tonwar,[11] J.Tóth,[14] G.Trowitzsch,[52] C.Tully,[40] K.L.Tung,[7] J.Ulbricht,[53] M.Unger,[52] E.Valente,[42] H.Verkooijen,[2] R.T.Van de Walle,[33] R.Vasquez,[50] V.Veszpremi,[28] G.Vesztergombi,[14] I.Vetlitsky,[30] D.Vicinanza,[43] G.Viertel,[53] S.Villa,[41] M.Vivargent,[4] S.Vlachos,[5] I.Vodopianov,[28] H.Vogel,[38] H.Vogt,[52] I.Vorobiev,[38,30] A.A.Vorobyov,[37] M.Wadhwa,[5] R.G.Wang,[7] Q.Wang,[33] X.L.Wang,[24] X.W.Wang,[7] Z.M.Wang,[24] M.Weber,[20] R.van Wijk,[2] T.A.M.Wijnen,[33] H.Wilkens,[33] S.Wynhoff,[40] L.Xia,[35] Y.P.Xu,[53] J.S.Xu,[7] Z.Z.Xu,[24] B.Z.Yang,[24] C.G.Yang,[7] H.J.Yang,[3] M.Yang,[7] X.F.Yang,[7] Z.G.Yao,[53] S.C.Yeh,[49] Z.Q.Yu,[7] An.Zalite,[37] Yu.Zalite,[37] C.Zhang,[7] F.Zhang,[7] J.Zhang,[7] S.Zhang,[7] Z.P.Zhang,[24] J.Zhao,[24] S.J.Zhou,[7] G.Y.Zhu,[7] R.Y.Zhu,[35] Q.Q.Zhu,[7] H.L.Zhuang,[7] A.Zichichi,[10,20,21] B.Zimmermann,[53] M.Zöller,[1] A.N.M.Zwart.[2]

21

1 III. Physikalisches Institut, RWTH, D-52056 Aachen, Germany[§]
2 NIKHEF, and University of Amsterdam, NL-1009 DB Amsterdam, The Netherlands
3 University of Michigan, Ann Arbor, MI 48109, USA
4 LAPP,IN2P3-CNRS, BP 110, F-74941 Annecy-le-Vieux CEDEX, France
5 Institute of Physics, University of Basel, CH-4056 Basel, Switzerland
6 Louisiana State University, Baton Rouge, LA 70803, USA
7 Institute of High Energy Physics, IHEP, 100039 Beijing, China[△]
8 ITP, Academia Sinica, 100039 Beijing, China
9 Humboldt University, D-10115 Berlin, Germany.
10 University of Bologna and INFN-Sezione di Bologna, I-40126 Bologna, Italy
11 Tata Institute of Fundamental Research, Mumbai (Bombay) 400 005, India
12 Northeastern University, Boston, MA 02115, USA
13 Institute of Atomic Physics and University of Bucharest, R-76900 Bucharest, Romania
14 Central Research Institute for Physics of the Hungarian Academy of Sciences, H-1525 Budapest 114, Hungary[‡]
15 Massachusetts Institute of Technology, Cambridge, MA 02139, USA
16 Panjab University, Chandigarh 160 014, India
17 KLTE-ATOMKI, H-4010 Debrecen, Hungary[¶]
18 Department of Experimental Physics, University College Dublin, Belfield, Dublin 4, Ireland
19 University of Florence and INFN, Sezione di Firenze, I-50019 Sesto Fiorentino, Italy
20 European Laboratory for Particle Physics, CERN, CH-1211 Geneva 23, Switzerland
21 World Laboratory, FBLJA Project, CH-1211 Geneva 23, Switzerland
22 University of Geneva, CH-1211 Geneva 4, Switzerland
23 University of Hamburg, D-22761 Hamburg, Germany
24 Chinese University of Science and Technology, USTC, Hefei, Anhui 230 029, China[△]
25 University of Lausanne, CH-1015 Lausanne, Switzerland
26 Institut de Physique Nucléaire de Lyon, IN2P3-CNRS,Université Claude Bernard, F-69622 Villeurbanne, France
27 Centro de Investigaciones Energéticas, Medioambientales y Tecnológicas, CIEMAT, E-28040 Madrid, Spain[♭]
28 Florida Institute of Technology, Melbourne, FL 32901, USA
29 INFN-Sezione di Milano, I-20133 Milan, Italy
30 Institute of Theoretical and Experimental Physics, ITEP, Moscow, Russia
31 INFN-Sezione di Napoli and University of Naples, I-80125 Naples, Italy
32 Department of Physics, University of Cyprus, Nicosia, Cyprus
33 Radboud University and NIKHEF, NL-6525 ED Nijmegen, The Netherlands
34 Osaka City University, Osaka 558-8585, Japan
35 California Institute of Technology, Pasadena, CA 91125, USA
36 INFN-Sezione di Perugia and Università Degli Studi di Perugia, I-06100 Perugia, Italy
37 Nuclear Physics Institute, St. Petersburg, Russia
38 Carnegie Mellon University, Pittsburgh, PA 15213, USA
39 INFN-Sezione di Napoli and University of Potenza, I-85100 Potenza, Italy
40 Princeton University, Princeton, NJ 08544, USA
41 University of California, Riverside, CA 92521, USA
42 INFN-Sezione di Roma and University of Rome, "La Sapienza", I-00185 Rome, Italy
43 University and INFN, Salerno, I-84100 Salerno, Italy
44 University of California, San Diego, CA 92093, USA
45 University of Santiago de Compostela, E-15706 Santiago, Spain
46 Bulgarian Academy of Sciences, Central Lab. of Mechatronics and Instrumentation, BU-1113 Sofia, Bulgaria
47 The Center for High Energy Physics, Kyungpook National University, 702-701 Taegu, Republic of Korea
48 National Central University, Chung-Li, Taiwan, China
49 Department of Physics, National Tsing Hua University, Taiwan, China
50 Purdue University, West Lafayette, IN 47907, USA
51 Paul Scherrer Institut, PSI, CH-5232 Villigen, Switzerland
52 DESY, D-15738 Zeuthen, Germany
53 Eidgenössische Technische Hochschule, ETH Zürich, CH-8093 Zürich, Switzerland
§ Supported by the German Bundesministerium für Bildung, Wissenschaft, Forschung und Technologie.
‡ Supported by the Hungarian OTKA fund under contract numbers T019181, F023259 and T037350.
¶ Also supported by the Hungarian OTKA fund under contract number T026178.
♭ Supported also by the Comisión Interministerial de Ciencia y Tecnología.
♯ Also supported by CONICET and Universidad Nacional de La Plata, CC 67, 1900 La Plata, Argentina.
△ Supported by the National Natural Science Foundation of China.
⊙ On leave from the Moscow Physical Engineering Institute (MePhI).
◇ On leave from JINR, RU-141980 Dubna, Russia.
† Deceased
⊕ Corresponding author, e-mail: *Pierre.Le.Coultre@cern.ch*